Acta Biomaterialia 198 (2025) 291–301

Contents lists available at ScienceDirect

Acta Biomaterialia

journal homepage: www.elsevier.com/locate/actbio

Full length article

Contact-free characterization of nuclear mechanics using correlative Brillouin-Raman Micro-Spectroscopy in living cells

S. Kerdegari [a,b], A.A. Passeri [c], F. Morena [d], G. Ciccone [e,f], V. Bazzurro [a], P. Canepa [a], A. Lagomarsino [a], S. Martino [d], M. Mattarelli [c], M. Vassalli [f], A. Diaspro [a,b], S. Caponi [g,*], C. Canale [a,*]

[a] Department of Physics, University of Genova, Genova, Italy
[b] Istituto Italiano di Tecnologia, Genova, Italy
[c] Department of Physics and Geology, University of Perugia, Perugia, Italy
[d] Department of Chemistry, Biology, and Biotechnology, Perugia, Italy
[e] Institute for Bioengineering of Catalonia (IBEC), The Barcelona Institute for Science and Technology (BIST), Barcelona, Spain
[f] James Watt School of Engineering, University of Glasgow, Glasgow, UK
[g] Istituto Officina dei Materiali del CNR, (CNR-IOM) unità di Perugia, Italy

ARTICLE INFO

Keywords:
AFM
Brillouin microscopy
Raman spectroscopy
Nuclear mechanics
Mechanobiology

ABSTRACT

Nuclear mechanics is a key parameter in regulating cell physiology, affecting chromatin accessibility and transcriptional regulation. The most established method to characterize the mechanics of biological materials at the sub-micrometer scale is based on atomic force microscopy (AFM). However, its contact-based nature limits the direct access to the nucleus. While some indirect methods have been proposed to measure nuclear mechanics in living cells, the readout is influenced by the overlaying cytoskeleton. For this reason, mechanical measurements on isolated nuclei are a common strategy to overcome this issue. However, the impact of the invasive preparation procedure on the measured properties is still unclear. To address this issue, we studied the mechanical properties of skin fibroblasts probing the nuclear region and of extracted nuclei using AFM and correlative Brillouin-Raman Micro-Spectroscopy (BRMS). The latter technique is a non-invasive method to image living systems in 3D, obtaining correlative information on the mechanical and chemical properties of the sample at specific points of interest. Using this approach, we demonstrated that extracted nuclei are significantly softer than intact ones. Moreover, we demonstrated the ability of BRMS to highlight mechanical features within living cells that were masked by the convolution with the cytosol in conventional AFM measurements. Overall, this study shows the importance of evaluating nuclear mechanics within the native environment where cellular homeostasis is preserved. We, therefore, suggest that BRMS offers a much deeper insight into nuclear mechanics compared to AFM, and it should be adopted as a reference tool to study nuclear mechanobiology.

Statement of significance: The cell nucleus, the largest eukaryotic organelle, is crucial for cellular function and genetic material storage. Its mechanical properties, often altered in disease, influence key processes like chromatin accessibility. Although atomic force microscopy (AFM) is a standard method for studying nuclear mechanics, isolating nuclear stiffness in living cells is challenging due to interference from the cytoskeleton and plasma membrane. We demonstrate that correlative Brillouin-Raman Micro-Spectroscopy (BRMS) enables non-contact, high-resolution measurement of nuclear mechanics, capturing sub-micron details. We compare the results from BRMS with that obtained on the same samples with AFM. BRMS enhances our understanding of nuclear stiffness in physiological conditions, offering valuable insights for researchers in the field of mechanobiology, biotechnology, medicine, and bioengineering.

* Corresponding authors.
E-mail addresses: silvia.caponi@cnr.it (S. Caponi), claudio.canale@unige.it (C. Canale).

https://doi.org/10.1016/j.actbio.2025.04.009
Received 20 November 2024; Received in revised form 1 April 2025; Accepted 3 April 2025
Available online 4 April 2025

1. Introduction

Cells are subjected to various mechanical forces in their native environment, such as compression, tension, and shear [1–4]. Via mechanosensitive proteins, cells continuously sense these stimuli, responding with changes in shape, motility, differentiation, division, and overall gene expression [1,5–8]. Additionally, the response of cells to their mechanical microenvironment is directly reflected by adaptations in the cells' own mechanical properties [4,9,10]. The characterization of this process can have fundamental implications in tissue engineering [11–13], drug screening [8], and diagnosis of diseases and their treatments [14]. For this reason, cell mechanics is becoming recognized as a potential biomarker for identifying cellular states within the biophysical community [15].

The nucleus is a key determinant of a cell's mechanics, being the largest among the cell's organelles. While the nucleus was previously thought of solely as a container for genetic information, it is now recognized to have mechanosensitive properties that allow it to respond to external mechanical forces [16–18]. Whole cell mechanics has been deeply investigated in recent years, using a series of techniques and contributing to our current knowledge of the role of mechanics in cell physiology and pathology [19–21]. However, the available information on nuclear mechanics remains limited and measured by contact-based techniques, at times, contradictory. As highlighted in ref [22], the nucleus is usually considered the stiffest organelle [23–25], while in other studies, it is reported to be softer than the cytoskeleton [26–28]. Additionally, research suggests that the mechanical behavior of the nucleus depends on the deformation range: at low deformations, its properties are primarily influenced by chromatin, whereas at higher deformations, the nuclear lamina plays a dominant role [29]. Given that the nucleus is surrounded by the cytoskeleton, and more in general by a complex mechanical environment, [28,30,31], these inconsistencies are largely attributed to technical challenges in studying this organelle in its native cellular environment. The mechanisms by which force is transmitted, particularly across the nuclear envelope, and how forces regulate nucleoplasmic transport are still not fully understood [32,33], but it has been suggested that the stiffness of the nuclear envelope plays a key role in controlling how cellular forces impact chromatin organization and gene expression [33]. The nuclear envelope is a double-membrane structure that surrounds the nucleoplasm and is composed of inner and outer nuclear membranes. The inner nuclear membrane is connected to the nuclear lamina, a network of intermediate filament proteins that provides mechanical support to the nucleus. The nuclear lamina is responsible for the nuclear shape and mechanical stability [17]. Mutations in the proteins of the nuclear envelope, specifically lamins, result in a range of illnesses known as laminopathies [34], including Emery–Dreifuss muscular dystrophy, lipodystrophy, leukodystrophy, progeria, diabetes [26,35,36], as well as cancer cells [37–40]. Therefore, studying nuclear mechanics is of great importance for comprehending physio-pathological mechanisms and early diagnosis.

In cell mechanics, AFM is considered the gold standard method [41]. AFM has several key benefits, including i) achieving high levels of spatial resolution, ii) precise control over the forces applied, and iii) performing measurements in liquid environments that closely mimic physiological conditions [6]. However, in the study of nuclear stiffness, the AFM probe necessarily interacts with the cell membrane and with the cytosolic environment before reaching the nucleus, giving rise to a non-trivial problem in the decoupling of the contributions given by the different cell compartments to the mechanical measurements. Deconvolution methods and specialized probes have been proposed to infer the mechanical properties of the nucleus using AFM measurements [23,42], but the proposed approaches are numerically unstable and tricky to implement so that they have not been adopted by the scientific community. To overcome this issue, a procedure to isolate the cell's nucleus to directly study its mechanical properties has been proposed [26,35]. This method makes the nucleus directly accessible to the AFM probe, and it can offer interesting insights into physiology and pathology. However, this experimental protocol raises important questions on whether nuclear mechanics is preserved during extraction, due to the modified homeostasis and the lack of interaction with the surrounding cytoskeleton [43]. The researcher is faced with the dilemma: what is the actual stiffness of the nucleus? More generally, is there a method to characterize nuclear mechanics that avoids the invasive procedure of nucleus extraction?

To provide an answer to this question in this paper, AFM data obtained measuring the nuclear region of living cells, and the isolated conditions is compared with the data obtained using a correlative microscopy method integrating Brillouin and Raman microscopy (BRMS). Brillouin microscopy has recently emerged as a powerful tool for investigating cell mechanics [7,16,44–47], and the integration with Raman has opened for a whole new correlative representation of biological samples [48]. Brillouin microscopy (BM), based on light-matter interaction, offers a non-contact and label-free approach to analyzing the physical properties of the material. Although widely used in condensed matter physics, BM has only recently been applied to the analysis of biological materials, thanks to increased measurement speed [49] and the ability to reach subcellular spatial resolution [50,51]. Promising results have already been found in cell mechanics [16,44,52] as well as in tissue characterization [48,53], even in vivo [54–58].

In this study, the advantages of two different techniques, AFM and BRMS, are combined by integrating the information on Young's modulus and longitudinal modulus obtained from each method. We studied both nuclei in intact cells and isolated nuclei. All measurements indicate that the nuclei isolation procedure strongly affects nuclear mechanics.

2. Materials and methods

2.1. Cell culture

Human dermal fibroblasts cells (HDFa, ThermoFisher, C0135C) were cultured in flasks in the Dulbecco's Modified Eagle Medium (DMEM, Sigma-Aldrich, USA) with 10 % FBS (Fetal Bovine Serum), 2 mM glutamine, and 100 IU/mL penicillin-streptomycin (Sigma-Aldrich, St. Louis, MO, USA). Cells were maintained at 5 % CO_2 and 37 °C temperature in a standard incubator. When confluency was reached, cells were split and cultured in new flasks, not for more than 16 passages. For mechanical measurements, low density of cells were seeded in poly-L-lysine coated (20 μg/ml) Petri dishes (TPP Techno Plastic Products, Switzerland) to prevent them from overlapping. Prior to the measurements, cells were washed twice with Dulbecco's Phosphate-Buffered Saline (DPBS, Sigma-Aldrich, USA) with calcium chloride and magnesium chloride (Sigma-Aldrich D8662).

2.2. Nuclei isolation

Cells were incubated in a hypotonic solution of 0.56 % potassium chloride (KCl) at 37 °C to alter the osmotic pressure. After 60 min, the KCl solution was aspirated gently to avoid cell detachment, and cells were subsequently incubated at room temperature in 0.1 % Triton X-100 (Sigma-Aldritch, USA) in DPBS for 5min. After triton removal, cells were suspended in DPBS, pipetting several times, and transferred into a falcon, centrifuged for 5min at 500g. Finally, the supernatant aspired, and the nuclei pellets were resuspended in fresh DPBS, deposited on a poly-L-lysine coated (20 μg/ml) Petri dish (TPP Techno Plastic Products, Switzerland), and kept for 1-2 h at 4 °C to let them settle before the measurements. Extracted nuclei were studied with confocal microscopy as well, to define the effectiveness of the method and to verify the integrity of the nuclei and the absence of cytosolic debris.

2.3. Ionic Strength change

DPBS without calcium and magnesium was used as the base medium. Following the manufacturer's specifications (Sigma-Aldrich, USA), the appropriate amounts of calcium chloride ($CaCl_2$) and magnesium chloride ($MgCl_2$) were added to the buffer to achieve a final concentration of 0.133 g/L for $CaCl_2$ and 0.1 g/L for $MgCl_2$ in the standard medium. To prepare the modified media with varying ionic strengths, the concentrations were doubled for the high-ionic-strength medium and halved for the low-ionic-strength medium.

2.4. Immunofluorescence labeling and confocal microscopy

Samples were prepared in Petri dishes, washed twice with DPBS, fixed in 4 % paraformaldehyde (Sigma-Aldrich) for 15 min at room temperature, and, after being washed three times with DPBS solution, permeabilized with 0.1 % Triton X-100 (Sigma-Aldrich) for 5 min at room temperature.

Cells were labeled with Phalloidin FITC (1:200) for 45 min at room temperature, washed three times with DPBS, incubated with Hoechst (1:1000) for 15 min at room temperature, and, after a wash with DPBS, mounted with ProLong™ glass antifade mountant (Thermo Fischer Scientific).

For Isolated nuclei, the nuclei were fixed in 4 % paraformaldehyde (Sigma-Aldrich) for 15 min at room temperature, washed three times with DPBS solution, and incubated with 2 % BSA (Bovine Serum Albumin) for 30 min at room temperature for blocking non-specific sites. The samples were washed three times with DPBS and, for observing the preservation of the nuclear membrane in isolated nuclei, incubated with the primary monoclonal mouse antibody against Pan Lamin (AB20740, Abcam) at a concentration of 1:50 in 2 % BSA overnight at 4 °C. Nuclei were washed three times in DPBS and incubated at room temperature for 45 min with 1:200 secondary antibody anti-mouse conjugated with Atto 647N. After washing three times in DPBS, the nuclei were labeled with Phalloidin FITC (1:200) for 45 min at room temperature, washed three times with DPBS, incubated with Hoechst (1:1000) for 15 min at room temperature, and, after a wash with DPBS, mounted with ProLong™ glass antifade mountant (Thermo Fischer Scientific).

Confocal z-stack images of the samples were obtained by using a Stellaris-8 (Leica Microsystems, Germany) equipped with a white light laser, HyD detectors, and 100x/1.40 NA oil immersion objective of an inverted microscope.

For volume analysis of the nuclei, live cells nuclei were Labeled with NucSpot Live 650 Nuclear Stain (1:1000, Biotium) and incubated at 37 °C for 2 h. Following incubation, samples were washed once and imaged in DPBS. Isolated nuclei were labeled in DPBS, incubated at 4 °C for 2 h, and subsequently imaged in DPBS.

2.5. Atomic force microscopy

AFM studies were conducted employing a Nanowizard IV (Bruker, USA) AFM system integrated with an inverse optical microscope DMi8 (Leica microsystem, Germany) equipped with 40x, 10x objectives, and 10x ocular. Two different kinds of probes and cantilevers were used. First, silicon nitride triangular cantilevers equipped with a pyramidal tip (DNP-10, Bruker, USA) were employed as sharp indenters. The nominal spring constant was 0.06 N/m, the tip radius of curvature was 20 nm. Subsequently, nuclear elasticity was probed using spherical polystyrene beads (Ø 10 μm; Polysciences, USA) mounted on silicon tipless cantilevers TL1 (Nanosensors, Switzerland) with the nominal spring constant of 0.03 N/m. The actual spring constant of each cantilever was determined in situ, using the thermal noise method [59].

In studying the samples, the AFM probe was positioned on top of the nucleus with the aid of the inverted optical microscope. In indentation experiments, the maximum force applied was 5 nN on the nuclear region of living cells and 3 nN on the isolated nuclei. The tip speed was maintained constant to 5 μm/s in all the experiments. Measurements were taken only from cells that were standalone, without any neighboring or overlapping cells. In the case of isolated nuclei, only those visually checked to be free of the cytoplasmic matrix were measured. Measurements were carried out in DPBS (Sigma-Aldrich, USA) for not more than 2 h in the Petri dishes, which were mounted in a temperature-controlled holder, the Petri dish heater (Bruker, USA), and kept at 37 °C.

To analyze the data, two different models of contact mechanics were employed: the standard Hertz-Sneddon model for the spherical probe and the Bilodeau approximation for the pyramidal tip. Hertz-Sneddon models are valid for axisymmetric indenters; Bilodeau extended the Hertz-Sneddon theory to non-axisymmetric geometry, such as quadratic pyramids. Eqs. (1) and (2) below represent the Hertz-Sneddon model for a spherical indenter and the Bilodeau approximation for a quadratic pyramid, respectively.

$$F = \frac{4}{3}\frac{E\sqrt{R\delta^3}}{(1-\nu^2)} \tag{1}$$

$$F = 0.7453\frac{E}{1-\nu^2}\delta^2 \tan\alpha \tag{2}$$

Where F is the force applied, δ is the indentation, ν the Poisson's ratio for nucleus and cell, which was considered 0.5 as for an incompressible material [60], R is the indenter radius, and α is the half-face angle of the pyramid. When using a spherical probe to investigate isolated nuclei, in the Hertz model, R is adjusted to account for the contact area between two spheres (the nucleus and the probe). Therefore, the effective radius of curvature R used in Eq. (1) is replaced by $\frac{1}{R} = \frac{1}{R_1} + \frac{1}{R_2}$, where R_1 and R_2 are the radii of the nuclei and the probe, both considered to be equal to 5 μm.

The AFM was also used to obtain stress-relaxation measurements. In this approach, we used spherical polystyrene beads (Ø 10 μm; Polysciences, USA) attached to an NP-10 silicon nitride tipless cantilever (Bruker, USA) with a nominal spring constant of 0.24 N/m. A deformation of the sample is applied sharply, approaching the sample at a tip velocity of 30 μm/s. The force was tuned to have indentation around 1.5-2.0 μm; for this reason, the force applied to nuclei was smaller than that applied to living cells. Once the force setpoint is reached, the AFM Z-piezo is maintained in a fixed position, and the cantilever deflection is monitored in time. After the large deformation is applied, the redistribution of the water content within the nucleus is responsible for the shape remodeling that brings a decrease in the cantilever deflection [61].

2.6. Brillouin-Raman microscopy

A detailed description of the custom-made setup for the correlative Raman and Brillouin analysis is reported in [44], here in brief we report the principal characteristics and the relevant information on the data acquisition and data treatment. The experimental setup uses a single-mode Spectra-Physics Excelsior laser of $\lambda = 532$ nm wavelength. The same water immersion objective (UPLSAPO 60XW from Olympus) is used both for focusing the light on the sample and collecting the back-scattered light. For this study, the intensity of the laser beam was reduced to approximately 6mW at the sample to prevent photodamage on the living cells. The samples of the cells and nuclei were prepared on a cover glass and kept in the HBSS for almost 2 h of measurements.

The scattered light is spectrally separated by an edge filter [44], the long wavelength component (> 533 nm) is analyzed by a Raman spectrometer (RM- Horiba iHR320 Triax) and the short wavelength component by a Brillouin interferometer (HC-TFP2) in order to relate the biochemical information to the mechanical properties.

In the backscattering geometry chosen in the presented experimental settings, the Brillouin spectra are composed of two Brillouin peaks (Stokes and anti-Stokes peaks) equally shifted by the elastic component.

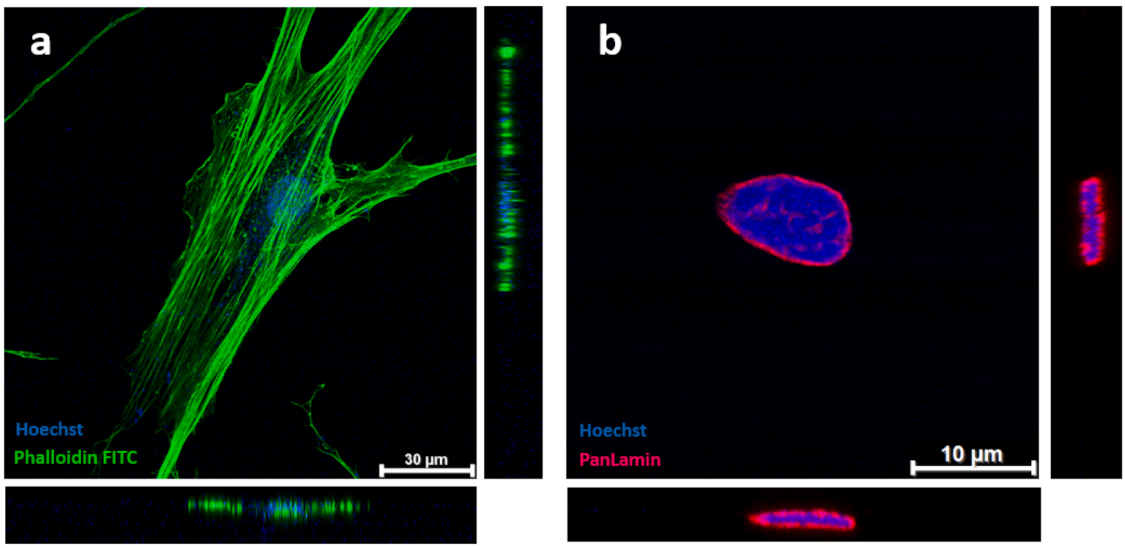

Fig. 1. a) Two-color confocal images of human skin fibroblast cells labeled with Phalloidin FITC for actin (green) and Hoechst for DNA (blue); the intact cell shows both signals, green and blue. b) isolated nuclei, labeled with the previous two fluorescent probes plus an additional anti-Pan Lamin antibody that binds Lamin A and Lamin B. The images show the isolated nuclei without the cytosol around them, and the nuclear lamina preserved.

The position and width of the Brillouin peaks contain information about the real and imaginary parts of the longitudinal elastic modulus.

$$\boldsymbol{M}\,(\boldsymbol{f}) = \boldsymbol{M}'\,(\boldsymbol{f}) + i\boldsymbol{M}''\,(\boldsymbol{f}) \tag{3}$$

In particular, the real part, M'(f), corresponding to the stiffness of the material at the Brillouin frequency, can be calculated by the frequency shift of the scattered light, while the imaginary part, M''(f) holds the information of the viscosity of the sample and it is related to the peak width, [7]. The real part which is of our interest can be given by:

$$M' = \frac{\rho f_B^2}{q^2} \tag{4}$$

Being q the exchanged wavevector of the scattering process

$$q = \frac{4\pi n}{\lambda}\sin\frac{\theta}{2} \tag{5}$$

Being ρ is the density, n the refractive index, and θ the angle between the illuminated and collected light. In our analysis, we considered a nuclear density of ρ = 1080 kg/m and a refractive index of n = 1.386, as reported in the literature [44,46]. These values have been kept constant for nuclei in both conditions. In fact, in the definition of the longitudinal elastic modulus, density, and refractive index are entered as ρ/n2, a ratio that, as highlighted in different cases in the literature, maintains a constant value [46,62,63]. From a physical standpoint, this approximation relies on the connection between the refractive index and density via atomic polarizability. In our analysis, we assumed that M′∝ ωb2 neglecting the variation in ρ/n2, which is less than 1 %, also in fibroblasts exposed to different levels of hyperosmotic shock [46]. The Brillouin spectrum is fitted using a DHO function convoluted with the instrumental response [44].

$$I(f) = \frac{\mathrm{I}_0}{\pi}\frac{f_B^2\Gamma}{\left(f^2 - f_B^2\right)^2 + f^2\Gamma^2} \otimes R(f) \tag{6}$$

f_B is extracted as a fitting parameter.

This method takes into account the spectral resolution of the spectrometer as well as the spread in q by the optical setting, i.e. all the possible q values allowed in the used optical configuration. For further details, refer to [44].

2.7. Statistical analysis

In this study, cells of six different passages were analyzed. AFM experiments measuring the Young's modulus of elasticity were performed on over 100 nuclei. For the BM, more than 60 nuclei and over 50 nucleoli were analyzed. Results are presented as the mean ± standard deviation (SD), calculated using OriginPro 2020. Statistical comparisons between the two groups were conducted using the Student's two-sample t-test. Statistical significance was denoted as follows: $p < 0.05$ (*); $p < 0.01$ (**); $p < 0.001$ (***); $p < 0.0001$ (****); and ns for no significant difference.

For comparisons involving longitudinal modulus versus Young's modulus, data are presented as the mean ± standard error of the mean (SEM) to be comparable with other papers.

3. Results and discussion

3.1. Intact cells and isolated nuclei

For the purpose of this study, with the aid of the inverted optical microscope of AFM only nuclei that were entirely free of cytosolic remnants were selected for measurement. However, to ensure a more precise analysis and to confirm the preservation of the Lamin region surrounding the nuclei, intact cells and isolated nuclei were labeled (Materials and Methods) and investigated by confocal microscopy. Images obtained from the intact cells show the nucleus in blue and the cytosol area in green (Fig. 1a). The confocal images taken after the nuclei isolation process reveal that the nucleus remains intact and is surrounded by the labeled nuclear lamina. It is important to note that the green signal of Phalloidin FITC is absent, indicating that the cytoplasmic matrix is completely removed after nuclei isolation (Fig. 1b).

3.2. AFM nanoindentation experiments

The AFM nanoindentation experiments were performed using both standard pyramid AFM probes and micro-sized spherical beads (Materials and Methods). With the aid of the inverted optical microscope, the AFM probe and nucleus are witnessed and marked. Fig. 2a, shows a spherical probe in the proximity of a living fibroblast. The nucleus (red circle) is clearly displayed in optical images; subsequently, the probe is positioned on top of the nuclear region of the cell to acquire the

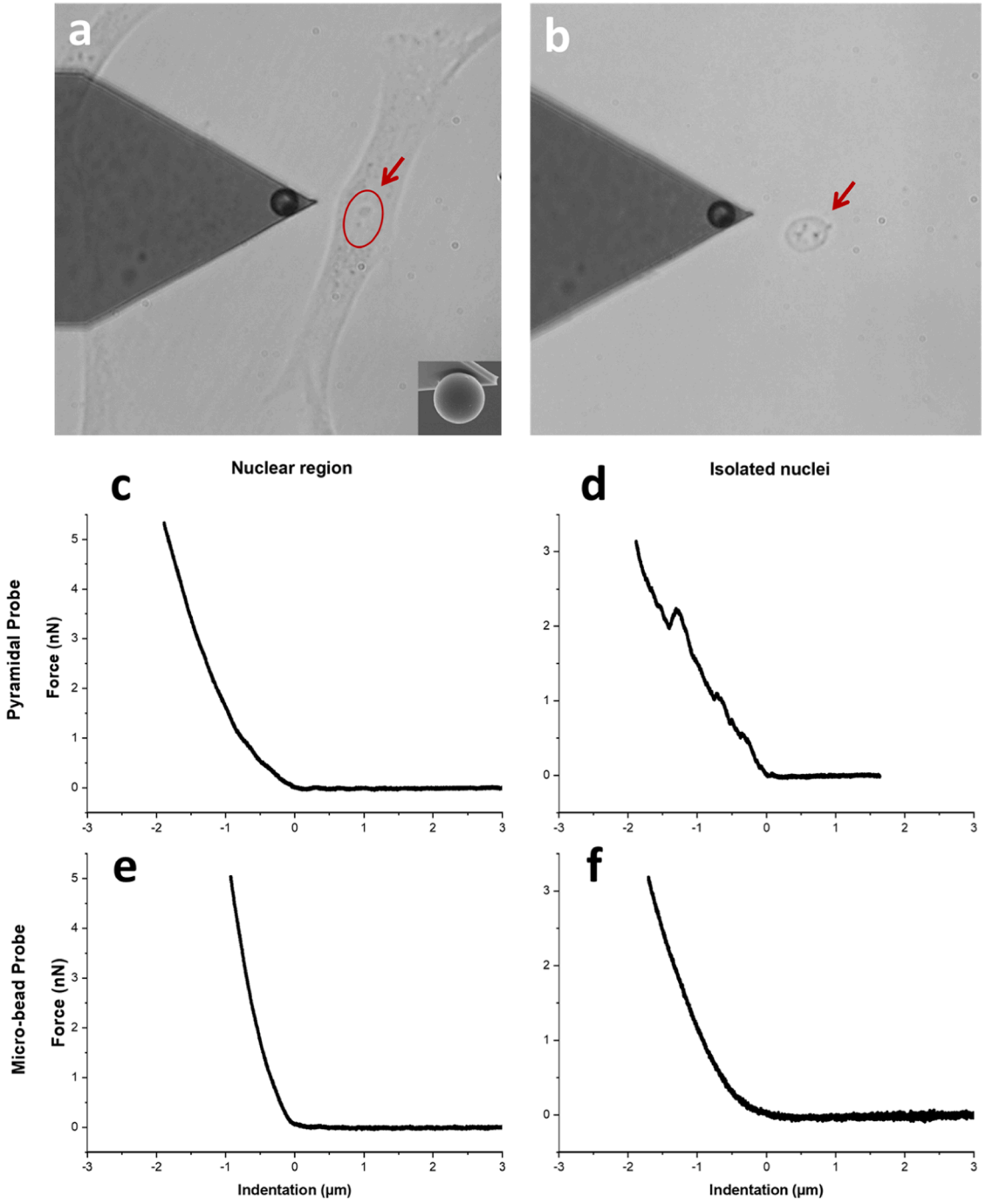

Fig. 2. a) The micro-bead probe and the nucleus in the living cell, marked by an arrow, the inset shows the SEM image of the probe b) the probe and the isolated nucleus c, d) force-indentation with the pyramidal sharp probe on the nuclear region of the cell and isolated nuclei respectively e, f) F-D curves of the micro-bead probe of the same samples.

corresponding force-distance (F-D) curve. Fig. 2b shows a spherical micro-bead probe and an isolated nucleus (red arrow).

F-D curves acquired on the nuclear region of living cells and isolated nuclei are reported (Fig. 2b,d–f). F-D curves obtained on the nuclear region of cells with sharp pyramidal probes resulted in a monotonic growth of F as a function of the indentation depth (Fig. 2c). On the contrary, curves acquired on isolated nuclei showed additional peaks, corresponding to tip penetration events (often multiple, Fig. 2d). This approach with specific AFM probes of a very high tip height was reported to study the nuclear mechanics [23], but for common pyramidal AFM probes used in this study, it is proposed that the cantilever might also come into contact with the cell for a certain amount of indentation; therefore pyramidal probes may overestimate E in comparison to spherical probes [64]. In this study, we are instead directly evaluating the nuclear region, which is the highest point, and the data were analyzed for lower forces and indentations before the breakthrough, lower than 600nm, an indentation depth well below the typical tip height in a pyramidal probe. Nonetheless, the experiments were continued using spherical microbeads. F-D curves acquired with larger indenters show a regular trend on both the nuclear region of living cells (Fig. 2e) and isolated nuclei (Fig. 2f).

Experiments with pyramid indenter were carried out on 192 nuclear

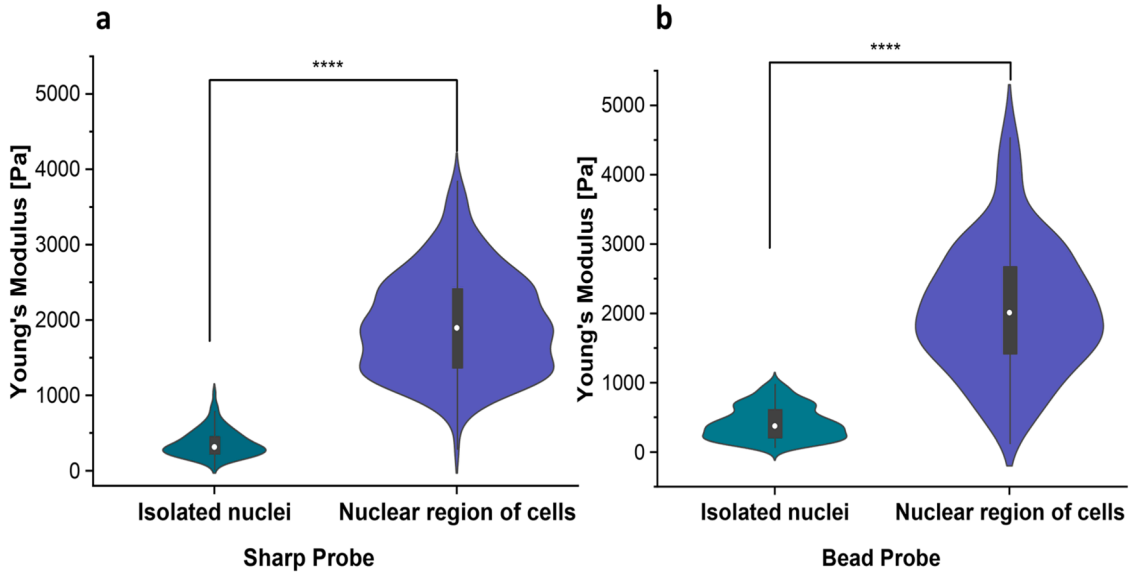

Fig. 3. Young's modulus of the isolated nuclei and nuclear region of living cells. a) Measurements with sharp probe show the isolated nuclei with an average of 370 ± 180 Pa is 4.8 times softer than the nuclear region of the living cell with an average of 1950 ± 660 Pa (****=$p < 0.0001$, two-sample t-test) b) Measurements with micro-bead probe shows the isolated nuclei with an average of 600 ± 300 Pa is 3.5 times softer than the nuclei in the living cell with an average of 2100 ± 900 Pa (****=$p < 0.0001$, two-sample t-test).

regions of living cells and 102 isolated nuclei, while spherical beads were carried out on 197 nuclear regions of living cells and 150 isolated nuclei from 6 different cell passages in culture. Comparison experiments provided different results: nuclei measured in their native environment, i.e., nuclear regions of living cells, appeared stiffer than the isolated nuclei by a factor of 3.5 in the case of micro-bead probe and by a factor of 4.8 in the case of pyramidal probes (Fig. 3). It needs to be mentioned that the results obtained with sharp pyramidal tips on isolated nuclei were not very reproducible, since also at indentation below 600 nm, one or more rupture events can be present in the F-D curves, being significant sources of indetermination. Only in this case, a significant number of curves have been rejected, due to their highly irregular behavior. The occurrence of breakthrough events indicates that isolated nuclear membranes are less resistant to mechanical stresses compared to the cell membrane. The nuclear membrane is made of a double lipid bilayer, stabilized by the presence of a filament meshwork of the nuclear lamina, but we do not have a-priori clues suggesting its poor mechanical stability. We cannot exclude that, although overcoming osmotic disruption, the lipid membrane of the nucleus can be damaged during isolation.

Other studies reported the influence of the cytoskeleton on nuclear mechanics due to the physical anchoring of the skeleton to the nucleus [27,28]. Furthermore, previous works demonstrated that the presence of the cytoskeleton is important in the regulation of nuclear mechanics and mechanotransduction [28,65,66]. In particular, actin and tubulin meshwork act by buffering external mechanical forces, reducing nuclear deformation, and aiding in strain recovery. This fact supports the idea

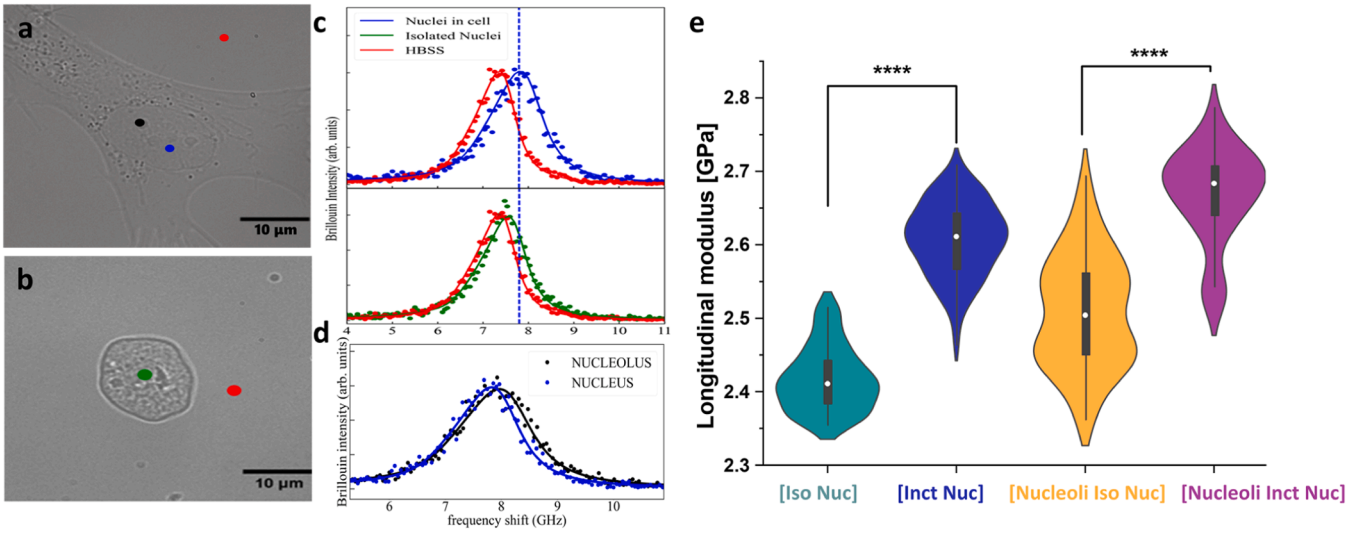

Fig. 4. a, b) Bright-field optical microscopy image of different points of measurement of the nucleus in a living cell, blue dot, isolated nucleus in green, nucleolus in black, and the buffer with red dot c) Brillouin peak of the nucleus in living cell and isolated nucleus in respect to the buffer marked by the dashed line, the fits are reported as solid lines while the data are the full dots d) Frequency shift of the nucleus in respect to nucleolus e) The Longitudinal modulus of the isolated nucleus [Iso Nuc], intact Nucleus in living cell [Inct Nuc], Nucleoli in the isolated nucleus [Nucleoli Iso Nuc], and nucleoli in intact Nucleus [Nucleoli Inct Nuc], form 93 intact cell and 68 number of isolated nuclei samples (**** = $p < 0.0001$, t-test). The elastic moduli were obtained considering a density of ρ = 1080 kg/m and a refractive index of n = 1.386 [44,46].

that isolated nuclei have different mechanics. We cannot exclude that the higher stiffness measured pushing on the nuclear area in living cells could be due to a spurious contribution provided by the rigid cytosolic region that is present between the nucleus and the AFM probe. The AFM analysis is not driving an unambiguous interpretation of the results. For this reason, the application of a second technique, possibly non-contact-based, is necessary to confirm this analysis.

3.3. Brillouin microscopy analysis

The simultaneous Raman and Brillouin Microscopy characterization enables the correlation of biochemical composition and mechanical properties by an all-optical approach. The typical Raman and Brillouin spectra acquired in the nucleus are compared to those of the buffer solution. While Brillouin spectra primarily provide information based on peak position and width, Raman spectra offer insights into the presence of specific chemical species and their relative concentrations through the presence of characteristic peaks and their intensities. Notably, in the high frequency range, there is a band centered around 2800 cm^{-1} in the Raman spectrum of the nucleus that corresponds to C-H_2 and C-H_3 stretching vibrations, indicating the presence of organic molecules such as lipids, proteins, and DNA [44]. The broad band centered at about 3300 cm^{-1} is attributed to the vibrational modes of water [44].

Although the BRMS technique allows high-resolution chemical and mechanical mapping, we prioritized analyzing a larger number of cells by examining multiple points within the nuclei. These points were randomly selected, while the nucleolar region, identified through bright-field imaging, was analyzed separately. To determine the optimal axial plane for measurements, a z-map signal of the Brillouin spectra was recorded at different focal planes, following the procedure described in ref [67]. The position was then chosen at the center of the nucleus.

By focusing the laser light inside the nucleus, it is possible to selectively measure nuclear mechanics within intact cells avoiding contributions of the surrounding cellular regions. The capability of BM to analyze small subcellular compartments is also tested by analyzing the nucleolus, a denser and smaller part of the nucleus with typical sizes ranging from 1-2 μm. Despite their relatively small size, nucleoli are significantly stiffer than other cellular structures, including the nucleus. Their properties have been already studied using BM and AFM [45,68,69]. The AFM study in ref [69], identified nucleoli in phase and amplitude images, but their mechanical properties were affected by the presence of fibers. Similarly, the BM study in ref [45] analyzed nucleoli. However, here we are focusing our interest on nuclear mechanics. The measured Brillouin spectra are reported in Fig. 4, comparing the signals of the nucleus in its native environment with those after the isolation process, together with the fitting curves and the buffer signal. Even in the raw data, the Brillouin peak shows a clear frequency shift occurring in isolated nuclei (Fig. 4c), this measurement unambiguously highlights the significant mechanical variation induced by the isolation process.

To quantify the mechanical modifications, we determined the longitudinal modulus for nuclei and nucleoli in intact cells and in isolated conditions. The data are plotted in Fig. 4e demonstrating that nuclei within the cell are significantly ($p < 0.0001$) stiffer than the isolated ones, exhibiting an increase in stiffness by a factor of 1.08. A comparable change is also measured for the nucleoli, attesting that the extraction procedure deeply alters nuclear mechanics, leading to modifications in the elasticity of these dense regions rich in genetic and protein material. The direct comparison between the stiffness measured by AFM and by Brillouin microscopy is not trivial, considering that the provided elastic moduli are fundamentally different [70]. While both of them measure the uniaxial strain response of the materials to the uniaxial stress, the longitudinal modulus (M) considers deformations constrained along the axis and measures the compliance of the sample to changes in volume. Instead, Young's modulus (E), considering unconstrained deformations, also measures the compliance of the sample to changes in shape even at constant or nearly constant volume [7,71].

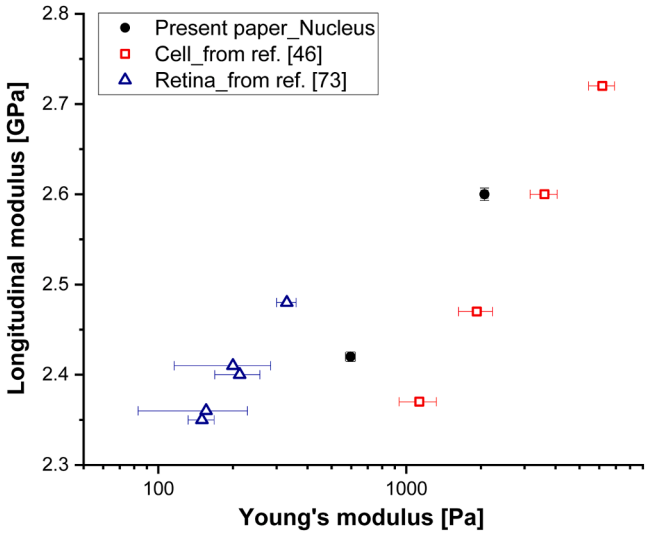

Fig. 5. a) Comparison of Young's modulus and the longitudinal modulus of the nuclei in two different microenvironments of intact cells and isolated. Young's modulus of elasticity shows 600 ± 300 Pa and 2100 ± 900 Pa for the isolated and intact nuclei, respectively; for the same samples, the longitudinal modulus is 2.41 ± 0.04 GPa and 2.59 ± 0.06 GPa. The plot shows mean and SEM. (black dots); the data of single cells from ref [46] are also reported for comparison together with the data of retina from ref [73] in which the Poisson ratio is fixed to the value of 0.5.

In fact, using the assumption of incompressible materials (Poisson ratio, $\nu = 0.5$), E is only sensitive to sample deformations and in this approximation often used for biological materials, the formal relation linking the longitudinal modulus, M, to Young's modulus, E,

$$M = E(1-\nu)/((1+\nu)(1-2\nu)),$$

leads to an undefined expression explaining why M and E differ by several orders of magnitude.

Moreover, as part of this fundamental difference, the Young's modulus measured by AFM and the longitudinal elastic modulus measured by Brillouin are also probed at very different frequency regimes (quasi-static and GHz, respectively). This is known to affect the elastic properties of biological samples, which have an intrisic viscoelastic nature [72]. In any case, despite these differences, experimental comparisons of M and E have been proposed for specific materials, such as cells under hyperosmotic shocks or different retinal layers [46,73], showing a positive correlation between them. Based on these empirical findings, the variation in M of 8 % measured in the present case can lead to a 3.5-fold modification in E.

In Fig. 5, we present the correlative variation between elastic moduli obtained by AFM and Brillouin microscopy. Even with the uncertainty due to the presence of other contributions in the AFM measurements, the observed variation in the two moduli appears to be consistent with the expected trend of litterature data.

4. Enriched water content in isolated nuclei modifies their mechanical properties

We found that the nuclear isolation procedure strongly modifies nuclear mechanics and that AFM nanoindentation reveals that the nuclear membrane does not withstand mechanical stresses induced by a sharp indenter (Fig. 2d). Additionally, the Raman spectra, acquired simultaneously with the Brillouin spectra, are examined to investigate the presence of eventual biochemical modifications induced by the isolation process. The analysis of Raman data (Fig. 6a) indicates a higher content of water in isolated nuclei with respect to the nuclei in living cells. Normalizing the Raman spectra at the high-frequency carbon-

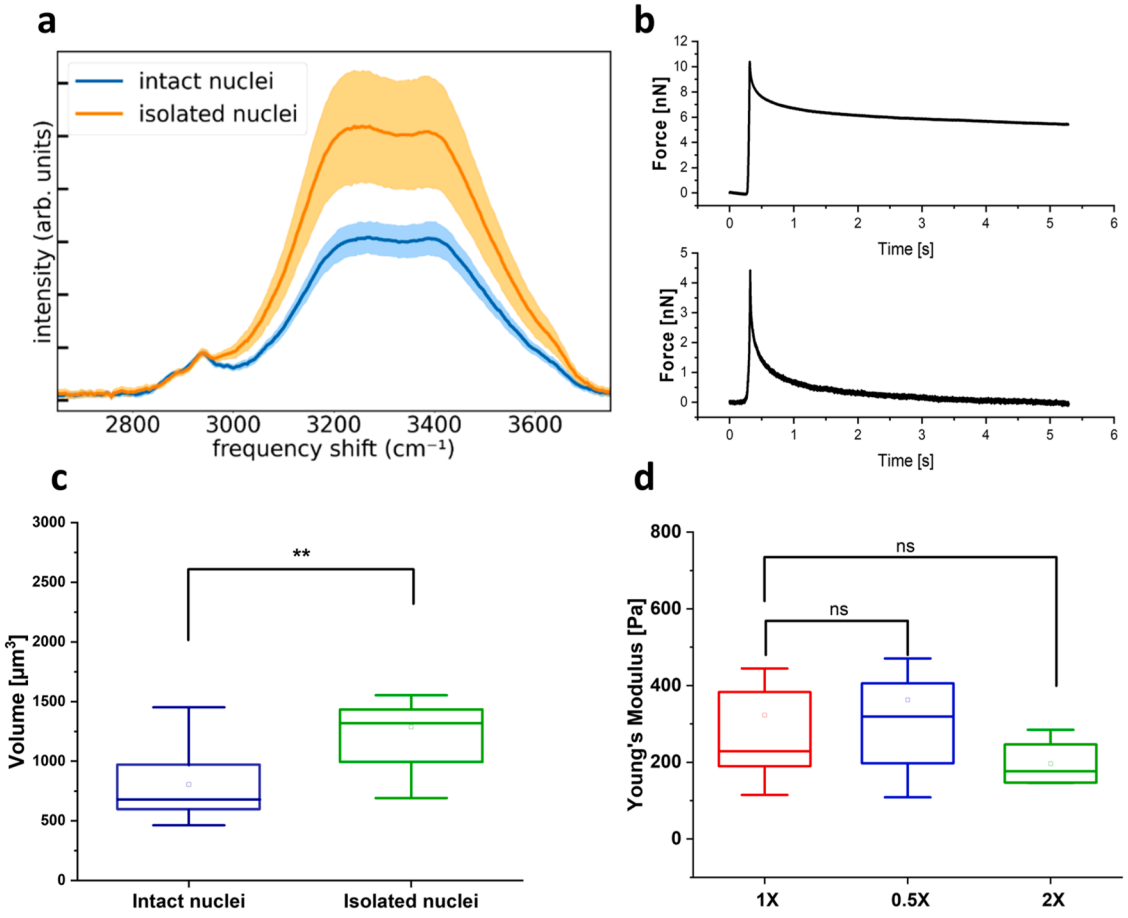

Fig. 6. a) High frequency of Raman spectra of isolated and intact nuclei. The spectra are normalized to the carbon-hydrogen (CH) stretching band, centered at about 2900 cm−1. The band centered at 3300 cm−1 is assigned to the OH stretching band of water. b) the F-T curve on the nuclear region of the living cell (top) and the corresponding F-T signal on the isolated nuclei (bottom). It shows that the applied force is going back close to zero after few seconds. c) The volume comparison of 19 nuclei in the two different microenvironments (two-sample t-test). d) Young's moduli of 15 isolated nuclei at different ionic strengths. 1x refers to the typical ionic concentration in PBS (two-sample t-test).

hydrogen (CH) stretching band, centered at about 2900 cm−1, the intensity of the OH band, centered at 3300 cm−1, is increased by a factor of 2.2.

While the intensity of the C-H stretching band can account for the dry mass present in the scattering volume, the intensity of the OH band is directly related to the water content, which is significantly higher in isolated nuclei with respect to the intact nuclei inside living cells. The data reveal significant changes in chemical composition, which may underlie the modified mechanical properties. To delve deeper inside, we applied a different AFM approach, acquiring stress-relaxation curves, as described in the Materials and Methods section. To acquire the stress-relaxation curves, we applied sharp deformation of the nuclei using large spherical indenters and applied forces that induced significant indentation (15 %-25 % of the overall nuclear thickness). After reaching the setpoint force, the Z-piezo is maintained in a fixed position for some seconds. The redistribution of the internuclear content is displayed by a decrease in the cantilever deflection (Fig. 6b) the deflection is reported in the force unit. On living cells, we found a typical visco-poroelastic behavior [22,61,74]. Qualitatively also, the curve on isolated nuclei follows this trend, but after a few seconds, the cantilever deflection reaches the same level observed in the baseline. Already 400 ms after reaching the setpoint force, the cantilever deflection is recovered for ~80 % while pushing on the nuclei within intact cells; this value is around 20 %. This anomalous behavior is related to the free motion of fluids through the nuclear membrane; the isolated nuclei membrane is not able to sustain hydrostatic pressure induced by the compressive forces, as in the case of the cell membrane.

To further investigate the increased water content of isolated nuclei, they were labeled and imaged using 3D confocal microscopy (Materials and methods). Nuclear volume was quantified using Fiji software and compared to that of nuclei in live cells and analyzed under the same conditions. The results, presented in Fig. 6c, indicate that the volume of isolated nuclei is indeed larger than that of intact nuclei, 1200 ± 500 μm^3 and 800 ± 300 μm^3 respectively, likely due to higher water content.

As a last examination, we studied nuclear mechanics, incubating the isolated nuclei in a buffer with different ionic strengths, following the procedure described in the Materials and Methods section. In principle, we expected an influx of water at low ionic strength and an outflux at high ionic strength. This should be the typical mechanism to reach the osmotic equilibrium in the presence of a semi-permeable membrane [75]. On the contrary, we found that the changes in buffer composition are not influencing the Young's modulus of the isolated nuclei (Fig. 6d).

The overall interpretation of these results is not obvious. The decreased capability of isolated nuclear membrane to withstand small indentation induced by AFM tip suggests a damage that compromises the membrane integrity. On the other hand, a decrease in stiffness in isolated nuclei was also measured using an isolation procedure that excludes the use of potentially damaging detergents [22]. Our additional experiments clearly indicate increased water content in isolated nuclei and the capability of water to freely diffuse through the nuclear membrane. However, it was already known that the membrane of the nucleus, characterized by the presence of the large gates represented by the

nuclear pore complexes, is permeable to water and even to relatively large macromolecules until ~40 kDa, and variation in the osmotic pressure, (in this case, more appropriately defined colloid osmotic pressure) have been measured only in the presence of macromolecules with molecular weight above 70 kDa [76,77]. The nuclear membrane is not behaving as a semi-permeable membrane but as a membrane selectively permeable to water and macromolecules below a certain size. The lack of macromolecules outside the isolated nucleus, results in a lower osmotic pressure from the external environment. This led to an influx of water into the nucleus causing swelling of the nucleus, within this larger nuclear volume, a loosening of chromatin packing occurs [78], finally contributing to lower stiffness of isolated nuclei as a consequence of the reduced macromolecular crowding.

5. Conclusion

In this research, a multi-technique approach was used for a comprehensive study of nuclear mechanics. We demonstrated how the use of an integrated approach, based on a combination of complementary techniques, improves our investigation capability and could be important to define new procedures to cover the gap between research applications and biomedical/diagnostic developments.

In our investigation, AFM and Brillouin Microscopy were employed to examine the nucleus in two different microenvironments: inside living cells and in isolated conditions. From AFM analysis isolated nuclei result significantly softer compared to those indented within living cells. Isolated nuclei are removed from their native environment, resulting in the loss of connections to the surrounding cytoskeleton. Conversely, studying the nucleus within a living cell using AFM which is a contact-based technique, cannot entirely eliminate potential contributions from the overlying cytoskeletal architecture. This limitation is not present in Brillouin Microscopy, which uses an all-optical microscopy approach. Brillouin Microscopy detected a significant decrease in the elasticity modulus of isolated nuclei, demonstrating that the nuclear extraction process strongly modifies nuclear mechanics. The results from the two techniques are in agreement, indicating that particular attention must be paid to results obtained from isolated nuclei. Despite this, the isolated nuclei can still be used for comparative experiments, such as comparing the stiffnesses of different populations of nuclei, as done by Ferrera et al. [35]. Further evidence revealed an increased water content in isolated nuclei. The altered nuclear homeostasis, together with the loss of contact with other cytosolic structures are at the base of the changes of their mechanical properties.

In conclusion, an accurate evaluation of the mechanical properties of the nucleus can be done only by working on living cells, avoiding the loss of physical connection with the cytoskeletal structures and probable modification of the nuclear membrane properties. To this end, using BRMS for measuring nuclear mechanics is suggested thanks to its capability to precisely localize the analysis in a subcellular volume without the use of a physical probe.

CRediT authorship contribution statement

S. Kerdegari: Writing – review & editing, Writing – original draft, Methodology, Investigation, Data curation. **A.A. Passeri:** Writing – review & editing, Writing – original draft, Investigation, Data curation. **F. Morena:** Writing – review & editing, Writing – original draft, Investigation. **G. Ciccone:** Writing – review & editing, Writing – original draft, Software, Methodology. **V. Bazzurro:** Investigation. **P. Canepa:** Investigation. **A. Lagomarsino:** Software, Methodology. **S. Martino:** Writing – review & editing, Writing – original draft, Supervision, Conceptualization. **M. Mattarelli:** Writing – review & editing, Writing – original draft, Supervision, Methodology, Conceptualization. **M. Vassalli:** Writing – review & editing, Writing – original draft, Software, Conceptualization. **A. Diaspro:** Conceptualization. **S. Caponi:** Writing – review & editing, Writing – original draft, Supervision, Funding acquisition, Conceptualization. **C. Canale:** Writing – review & editing, Writing – original draft, Supervision, Methodology, Funding acquisition, Conceptualization.

Declaration of competing interest

The authors declare that they have no known competing financial interests or personal relationships that could have appeared to influence the work reported in this paper.

Acknowledgments

We thank Dr. C.Argentati, from the University of Perugia for technical support. This work has been partially funded by the European Union - NextGenerationEU under the Italian Ministry of University and Research (MUR) National Innovation Ecosystem (grant ECS00000041 - VITALITY - CUP J97G22000170005 and CUP B43C22000470005); the European Union – NextGeneration EU (Prin PNRR grant P2022RH4HH - COMBINE-CUP B53D2302864 0001, by Italian Ministry of University and Research (MUR), National Recovery and Resilience Plan (NRRP), project MNESYS (PE0000006)—A Multiscale integrated approach to the study of the nervous system in health and disease (DN. 1553 11.10.2022); PRIN-PNRR BIOFORTE - CUP 1: J53D23015610001, Italian Ministry of University and Research (MUR), grant (P20225MR3), and by Molecular Scale Biophysics Research Infrastructure (MOSBRI, grant agreement number: 101004806—H2020-INFRAIA-2018-2020/H2020-INFRAIA-2020-1). SEELIFE ("StrEngthEning the ItaLIan InFrastructure of Euro-bioimaging") funded by the EU - Next Generation PNRR MUR Infrastructure program (B53C22001810006, IR0000023).

References

[1] H. Abuwarda, M.M. Pathak, Mechanobiology of neural development, Curr. Opin. Cell Biol. 66 (2020) 104–111.
[2] E.B. Dolan, S.W. Verbruggen, R.A. Rolfe, Techniques for studying mechanobiology, Mechanobiol. Health Disease (2018) 1–53.
[3] P. Prendergast, R. Huiskes, K. Søballe, Biophysical stimuli on cells during tissue differentiation at implant interfaces, J. Biomech. 30 (6) (1997) 539–548.
[4] P.-H. Wu, D.R.-B. Aroush, A. Asnacios, W.-C. Chen, M.E. Dokukin, B.L. Doss, P. Durand-Smet, A. Ekpenyong, J. Guck, N.V. Guz, A comparison of methods to assess cell mechanical properties, Nat. Methods 15 (7) (2018) 491–498.
[5] K. Beicker, E.T. O'Brien, M.R. Falvo, R. Superfine, Vertical light sheet enhanced side-view imaging for AFM cell mechanics studies, Sci. Rep. 8 (1) (2018) 1–12.
[6] A. Rigato, Characterization of Cell Mechanics with Atomic Force Microscopy: Mechanical Mapping and High-speed Microrheology, Aix-Marseille, 2015.
[7] R. Prevedel, A. Diz-Muñoz, G. Ruocco, G. Antonacci, Brillouin microscopy: an emerging tool for mechanobiology, Nat. Methods 16 (10) (2019) 969–977.
[8] R. Krishnan, J.-A. Park, C.Y. Seow, P.V. Lee, A.G. Stewart, Cellular biomechanics in drug screening and evaluation: mechanopharmacology, Trends Pharmacol. Sci. 37 (2) (2016) 87–100.
[9] I. Tortorella, C. Argentati, C. Emiliani, F. Morena, S. Martino, Biochemical pathways of cellular mechanosensing/mechanotransduction and their role in neurodegenerative diseases pathogenesis, Cells 11 (19) (2022) 3093.
[10] I. Tortorella, C. Argentati, C. Emiliani, S. Martino, F. Morena, The role of physical cues in the development of stem cell-derived organoids, Eur. Biophys. J. (2022) 1–13.
[11] T.L. Jenkins, D. Little, Synthetic scaffolds for musculoskeletal tissue engineering: cellular responses to fiber parameters, NPJ Regenerat. Med. 4 (1) (2019) 15.
[12] L. Donati, M.L. Valicenti, S. Giannoni, F. Morena, S. Martino, Biomaterials mimicking mechanobiology: a specific design for a specific biological application, Int. J. Mol. Sci. 25 (19) (2024) 10386.
[13] S. Kim, M. Uroz, J.L. Bays, C.S. Chen, Harnessing mechanobiology for tissue engineering, Dev. Cell 56 (2) (2021) 180–191.
[14] W. Yu, S. Sharma, J.K. Gimzewski, J. Rao, Nanocytology as a potential biomarker for cancer, Biomark. Med. 11 (3) (2017) 213–216.
[15] D. Di Carlo, A mechanical biomarker of cell state in medicine, J. Laborat. Autom. 17 (1) (2012) 32–42.
[16] J. Zhang, F. Alisafaei, M. Nikolić, X.A. Nou, H. Kim, V.B. Shenoy, G. Scarcelli, Nuclear mechanics within intact cells is regulated by cytoskeletal network and internal nanostructures, Small 16 (18) (2020) 1907688.
[17] J. Lammerding, Mechanics of the nucleus, Comprehens. Physiol. 1 (2) (2011) 783.
[18] Y. Kalukula, A.D. Stephens, J. Lammerding, S. Gabriele, Mechanics and functional consequences of nuclear deformations, Nat. Rev. Mol. Cell Biol. 23 (9) (2022) 583–602.
[19] G. Coceano, M. Yousafzai, W. Ma, F. Ndoye, L. Venturelli, I. Hussain, S. Bonin, J. Niemela, G. Scoles, D. Cojoc, Investigation into local cell mechanics by atomic

force microscopy mapping and optical tweezer vertical indentation, Nanotechnology 27 (6) (2015) 065102.
[20] B. González-Bermúdez, G.V. Guinea, G.R. Plaza, Advances in micropipette aspiration: applications in cell biomechanics, models, and extended studies, Biophys. J. 116 (4) (2019) 587–594.
[21] H.G. Lim, H.-C. Liu, C.W. Yoon, H. Jung, M.G. Kim, C. Yoon, H.H. Kim, K.K. Shung, Investigation of cell mechanics using single-beam acoustic tweezers as a versatile tool for the diagnosis and treatment of highly invasive breast cancer cell lines: an in vitro study, Microsyst. Nanoengineer. 6 (1) (2020) 39.
[22] Y.M. Efremov, S.L. Kotova, A.A. Akovantseva, P.S. Timashev, Nanomechanical properties of enucleated cells: contribution of the nucleus to the passive cell mechanics, J. Nanobiotechnol. 18 (2020) 1–11.
[23] H. Liu, J. Wen, Y. Xiao, J. Liu, S. Hopyan, M. Radisic, C.A. Simmons, Y. Sun, In situ mechanical characterization of the cell nucleus by atomic force microscopy, ACS nano 8 (4) (2014) 3821–3828.
[24] N. Caille, O. Thoumine, Y. Tardy, J.-J. Meister, Contribution of the nucleus to the mechanical properties of endothelial cells, J. Biomech. 35 (2) (2002) 177–187.
[25] F. Guilak, J.R. Tedrow, R. Burgkart, Viscoelastic properties of the cell nucleus, Biochem. Biophys. Res. Commun. 269 (3) (2000) 781–786.
[26] K. Apte, R. Stick, M. Radmacher, Mechanics in human fibroblasts and progeria: lamin A mutation E145K results in stiffening of nuclei, J. Mol. Recognit. 30 (2) (2017) e2580.
[27] T. Sugitate, T. Kihara, X.-Y. Liu, J. Miyake, Mechanical role of the nucleus in a cell in terms of elastic modulus, Curr. Appl Phys. 9 (4) (2009) e291–e293.
[28] X. Wang, H. Liu, M. Zhu, C. Cao, Z. Xu, Y. Tsatskis, K. Lau, C. Kuok, T. Filleter, H. McNeill, Mechanical stability of the cell nucleus–roles played by the cytoskeleton in nuclear deformation and strain recovery, J. Cell Sci. 131 (13) (2018) jcs209627.
[29] C.M. Hobson, M. Kern, E.T. O'Brien III, A.D. Stephens, M.R. Falvo, R. Superfine, Correlating nuclear morphology and external force with combined atomic force microscopy and light sheet imaging separates roles of chromatin and lamin A/C in nuclear mechanics, Mol. Biol. Cell 31 (16) (2020) 1788–1801.
[30] D. Tremblay, L. Andrzejewski, A. Leclerc, A.E. Pelling, Actin and microtubules play distinct roles in governing the anisotropic deformation of cell nuclei in response to substrate strain, Cytoskeleton 70 (12) (2013) 837–848.
[31] F. Houben, F. Ramaekers, L. Snoeckx, J. Broers, Role of nuclear lamina-cytoskeleton interactions in the maintenance of cellular strength, Biochim. Biophys. Acta 1773 (5) (2007) 675–686.
[32] I. Andreu, I. Granero-Moya, N.R. Chahare, K. Clein, M. Molina-Jordán, A.E. Beedle, A. Elosegui-Artola, J.F. Abenza, L. Rossetti, X. Trepat, Mechanical force application to the nucleus regulates nucleocytoplasmic transport, Nat. Cell Biol. 24 (6) (2022) 896–905.
[33] K.N. Dahl, S.M. Kahn, K.L. Wilson, D.E. Discher, The nuclear envelope lamina network has elasticity and a compressibility limit suggestive of a molecular shock absorber, J. Cell Sci. 117 (Pt 20) (2004) 4779–4786.
[34] K. Haase, A.E. Pelling, Investigating cell mechanics with atomic force microscopy, J. R. Soc., Interface 12 (104) (2015) 20140970.
[35] D. Ferrera, C. Canale, R. Marotta, N. Mazzaro, M. Gritti, M. Mazzanti, S. Capellari, P. Cortelli, L. Gasparini, Lamin B1 overexpression increases nuclear rigidity in autosomal dominant leukodystrophy fibroblasts, FASEB J. 28 (9) (2014) 3906–3918.
[36] X. Mu, C. Tseng, W.S. Hambright, P. Matre, C.Y. Lin, P. Chanda, W. Chen, J. Gu, S. Ravuri, Y. Cui, Cytoskeleton stiffness regulates cellular senescence and innate immune response in Hutchinson–Gilford Progeria Syndrome, Aging Cell 19 (8) (2020) e13152.
[37] M. Zwerger, C.Y. Ho, J. Lammerding, Nuclear mechanics in disease, Annu. Rev. Biomed. Eng. 13 (2011) 397.
[38] S.S. Deville, N. Cordes, The extracellular, cellular, and nuclear stiffness, a trinity in the cancer resistome—a review, Front. Oncol. 9 (2019) 1376.
[39] T. Fischer, A. Hayn, C.T. Mierke, Effect of nuclear stiffness on cell mechanics and migration of human breast cancer cells, Front. Cell Dev. Biol. 8 (2020) 393.
[40] E. Frittoli, A. Palamidessi, F. Iannelli, F. Zanardi, S. Villa, L. Barzaghi, H. Abdo, V. Cancila, G.V. Beznoussenko, G.Della Chiara, Tissue fluidification promotes a cGAS–STING cytosolic DNA response in invasive breast cancer, Nat. Mater. (2022) 1–12.
[41] M. Krieg, G. Fläschner, D. Alsteens, B.M. Gaub, W.H. Roos, G.J. Wuite, H.E. Gaub, C. Gerber, Y.F. Dufrêne, D.J. Müller, Atomic force microscopy-based mechanobiology, Nat. Rev. Phys. 1 (1) (2019) 41–57.
[42] C. Roduit, S. Sekatski, G. Dietler, S. Catsicas, F. Lafont, S. Kasas, Stiffness tomography by atomic force microscopy, Biophys. J. 97 (2) (2009) 674–677.
[43] J.J. Romero, M.C. De Rossi, C. Oses, C.V. Echegaray, P. Verneri, M. Francia, A. Guberman, V. Levi, Nucleus-cytoskeleton communication impacts on OCT4-chromatin interactions in embryonic stem cells, BMC Biol. 20 (1) (2022) 1–17.
[44] S. Mattana, M. Mattarelli, L. Urbanelli, K. Sagini, C. Emiliani, M.D. Serra, D. Fioretto, S. Caponi, Non-contact mechanical and chemical analysis of single living cells by microspectroscopic techniques, Light: Sci. Appl. 7 (2) (2018), 17139-17139.
[45] G. Antonacci, S. Braakman, Biomechanics of subcellular structures by non-invasive Brillouin microscopy, Sci. Rep. 6 (1) (2016) 1–6.
[46] G. Scarcelli, W.J. Polacheck, H.T. Nia, K. Patel, A.J. Grodzinsky, R.D. Kamm, S. H. Yun, Noncontact three-dimensional mapping of intracellular hydromechanical properties by Brillouin microscopy, Nat. Methods 12 (12) (2015) 1132–1134.
[47] I. Kabakova, J. Zhang, Y. Xiang, S. Caponi, A. Bilenca, J. Guck, G. Scarcelli, Brillouin microscopy, Nature Rev. Methods Primers 4 (1) (2024) 8.
[48] M. Alunni Cardinali, A. Di Michele, M. Mattarelli, S. Caponi, M. Govoni, D. Dallari, S. Brogini, F. Masia, P. Borri, W. Langbein, Brillouin–Raman microspectroscopy for the morpho-mechanical imaging of human lamellar bone, J. R. Soc., Interface 19 (187) (2022) 20210642.
[49] J. Zhang, M. Nikolic, K. Tanner, G. Scarcelli, Rapid biomechanical imaging at low irradiation level via dual line-scanning Brillouin microscopy, Nat. Methods 20 (5) (2023) 677–681.
[50] M. Mattarelli, M. Vassalli, S. Caponi, Relevant length scales in Brillouin imaging of biomaterials: the interplay between phonons propagation and light focalization, ACS Photonics 7 (9) (2020) 2319–2328.
[51] A. Passeri, A. Di Michele, I. Neri, F. Cottone, D. Fioretto, M. Mattarelli, S. Caponi, Size and environment: The effect of phonon localization on micro-Brillouin imaging, Biomaterials Advances 147 (2023) 213341.
[52] V. Mahajan, T. Beck, P. Gregorczyk, A. Ruland, S. Alberti, J. Guck, C. Werner, R. Schlüßler, A.V. Taubenberger, Mapping tumor spheroid mechanics in dependence of 3D microenvironment stiffness and degradability by Brillouin microscopy, Cancers 13 (21) (2021) 5549.
[53] R. Mercatelli, S. Mattana, L. Capozzoli, F. Ratto, F. Rossi, R. Pini, D. Fioretto, F. S. Pavone, S. Caponi, R. Cicchi, Morpho-mechanics of human collagen superstructures revealed by all-optical correlative micro-spectroscopies, Commun. Biol. 2 (1) (2019) 117.
[54] C. Bevilacqua, H. Sánchez-Iranzo, D. Richter, A. Diz-Muñoz, R. Prevedel, Imaging mechanical properties of sub-micron ECM in live zebrafish using Brillouin microscopy, Biomed. Optics Express 10 (3) (2019) 1420–1431.
[55] R. Schlüßler, S. Möllmert, S. Abuhattum, G. Cojoc, P. Müller, K. Kim, C. Möckel, C. Zimmermann, J. Czarske, J. Guck, Mechanical mapping of spinal cord growth and repair in living zebrafish larvae by Brillouin imaging, Biophys. J. 115 (5) (2018) 911–923.
[56] P. Shao, A.M. Eltony, T.G. Seiler, B. Tavakol, R. Pineda, T. Koller, T. Seiler, S.-H. Yun, Spatially-resolved Brillouin spectroscopy reveals biomechanical abnormalities in mild to advanced keratoconus in vivo, Sci. Rep. 9 (1) (2019) 7467.
[57] P. Pruidze, E. Chayleva, W.J. Weninger, K. Elsayad, Brillouin scattering spectroscopy for studying human anatomy: Towards in situ mechanical characterization of soft tissue, J. Eur. Optical Society 19 (1) (2023).
[58] F. Yang, C. Bevilacqua, S. Hambura, A. Neves, A. Gopalan, K. Watanabe, M. Govendir, M. Bernabeu, J. Ellenberg, A. Diz-Muñoz, Pulsed stimulated Brillouin microscopy enables high-sensitivity mechanical imaging of live and fragile biological specimens, Nat. Methods 20 (12) (2023) 1971–1979.
[59] J.L. Hutter, J. Bechhoefer, Calibration of atomic-force microscope tips, Rev. Sci. Instrum. 64 (7) (1993) 1868–1873.
[60] G.H. Staab, 2 - A review of stress–strain and material behavior, in: G.H. Staab (Ed.), Laminar Composites (Second Edition), Butterworth-Heinemann 2015, pp. 17-36.
[61] E. Moeendarbary, L. Valon, M. Fritzsche, A.R. Harris, D.A. Moulding, A. J. Thrasher, E. Stride, L. Mahadevan, G.T. Charras, The cytoplasm of living cells behaves as a poroelastic material, Nat. Mater. 12 (3) (2013) 253–261.
[62] G. Scarcelli, R. Pineda, S.H. Yun, Brillouin optical microscopy for corneal biomechanics, Invest. Ophthalmol. Vis. Sci. 53 (1) (2012) 185–190.
[63] M. Bailey, M. Alunni-Cardinali, N. Correa, S. Caponi, T. Holsgrove, H. Barr, N. Stone, C.P. Winlove, D. Fioretto, F. Palombo, Brillouin-derived viscoelastic parameters of hydrogel tissue models, arXiv Preprint (2019) arXiv:1912.08292.
[64] R. Vargas-Pinto, H. Gong, A. Vahabikashi, M. Johnson, The effect of the endothelial cell cortex on atomic force microscopy measurements, Biophys. J. 105 (2) (2013) 300–309.
[65] M.C. Keeling, L.R. Flores, A.H. Dodhy, E.R. Murray, N. Gavara, Actomyosin and vimentin cytoskeletal networks regulate nuclear shape, mechanics and chromatin organization, Sci. Rep. 7 (1) (2017) 5219.
[66] A.-B. Ndiaye, G.H. Koenderink, M. Shemesh, Intermediate filaments in cellular mechanoresponsiveness: mediating cytoskeletal crosstalk from membrane to nucleus and back, Front. Cell Dev. Biol. 10 (2022) 882037.
[67] A.A. Passeri, C. Argentati, F. Morena, F. Bonacci, I. Neri, D. Fioretto, M. Vassalli, S. Martino, M. Mattarelli, S. Caponi, Brillouin spectroscopy for accurate assessment of morphological and mechanical characteristics in micro-structured samples, J. Phys.: Photonics (2024).
[68] C.R. Guerrero, P.D. Garcia, R. Garcia, Subsurface imaging of cell organelles by force microscopy, ACS nano 13 (8) (2019) 9629–9637.
[69] Y.M. Efremov, D.M. Suter, P.S. Timashev, A. Raman, 3D nanomechanical mapping of subcellular and sub-nuclear structures of living cells by multi-harmonic AFM with long-tip microcantilevers, Sci. Rep. 12 (1) (2022) 529.
[70] S. Caponi, A. Passeri, G. Capponi, D. Fioretto, M. Vassalli, M. Mattarelli, Non-contact elastography methods in mechanobiology: a point of view, Eur. Biophys. J. 51 (2) (2022) 99–104.
[71] M. Nikolić, C. Conrad, J. Zhang, G. Scarcelli, Noninvasive imaging: Brillouin confocal microscopy, Biomechan. Oncol. (2018) 351–364.
[72] K. Franze, P.A. Janmey, J. Guck, Mechanics in neuronal development and repair, Annu. Rev. Biomed. Eng. 15 (1) (2013) 227–251.
[73] I.P. Weber, S.H. Yun, G. Scarcelli, K. Franze, The role of cell body density in ruminant retina mechanics assessed by atomic force and Brillouin microscopy, Phys. Biol. 14 (6) (2017) 065006.
[74] Y.H. Chim, L.M. Mason, N. Rath, M.F. Olson, M. Tassieri, H. Yin, A one-step procedure to probe the viscoelastic properties of cells by Atomic Force Microscopy, Sci. Rep. 8 (1) (2018) 14462.
[75] P. Chengappa, K. Sao, T.M. Jones, R.J. Petrie, Intracellular pressure: a driver of cell morphology and movement, Int. Rev. Cell Molecular Biol. 337 (2018) 185–211.

[76] J. Ma, W. Yang, Three-dimensional distribution of transient interactions in the nuclear pore complex obtained from single-molecule snapshots, Proc. Natl Acad. Sci. 107 (16) (2010) 7305–7310.
[77] V. Shahin, I.U. Kouzel, G. Rosso, I. Liashkovich, Nuclear envelope permeability barrier as a fast-response intracellular mechanostat, Adv. Sci. 6 (21) (2019) 1900709.
[78] T. Lebeaupin, R. Smith, S. Huet, The multiple effects of molecular crowding in the cell nucleus: from molecular dynamics to the regulation of nuclear architecture, Nuclear Architec. Dynamics (2018) 209–232.